Comparison of spatial organization in top-down- and membrane-aerated biofilms: a numerical study

A. Bell, Y. Aoi, A. Terada, S. Tsuneda and A. Hirata

Department of Chemical Engineering, Waseda University, Tokyo, Japan (E-mail: *andrew@akane.waseda.jp*)

Abstract The study of community structure in wastewater biofilms is made difficult by the slow growth rates and high environmental sensitivities of autotrophic nitrifiers. Simulations of such films can generate data quickly and without susceptibility to random environmental perturbation. This study uses a 2D cellular automaton model to compare the community structures of biofilms grown under top-down and membrane aeration conditions. This study found dramatic differences in community structure between the two approaches, most notably the emergence of a niche at the solid–biofilm interface that facilitates the growth of nitrite oxidizing bacteria.

Keywords Biological nitrogen removal; cellular automaton; MABR; simulation; spatial organization

Water Science & Technology **Vol 52 No 7 pp 173–180** © IWA Publishing 2005

Introduction

It is widely acknowledged that the community structure of microorganisms and their spatial organization in biofilms used for wastewater treatment are important factors to be understood, and recent application of molecular techniques such as fluorescence in situ hybridization (FISH) have contributed greatly to our understanding of ecological function in laboratory and industrial biofilms. Aoi *et al*. (2000), Schramm *et al.* (1996) and Okabe *et al.* (1999) applied FISH to nitrifying biofilms and found vertical profiles in nitrifying activity that correlated with spatial organization of ammonia-oxidizing (AOB) and nitrite-oxidizing bacteria (NOB) in the film. Ecological study is limited, however, by the space, nutrient, and time requirements to grow the films for periods sufficiently long to gather meaningful data. Autotrophic nitrifying biofilms in particular are characterized by long growth times and sensitivity to environmental instabilities. Simulations can play a large role in such research, since they are not subject to random environmental perturbation, and as technology progresses, are less and less bound by time. In this study, we use a simple two-dimensional model to look at the differences in spatial organization of bacteria that arise from the qualitative differences of *top-down* and *membrane-aeration* approaches to biofilm growth. In nitrogen removal systems, lithoautotrophic nitrifiers and heterotrophic denitrifiers each have unique roles in the transformation of NH_3 to N_2 via NO_2^- and NO_3^-, making an understanding of their structure and organization important.

Conventional nitrogen removal systems consist of a separate nitrification and denitrification step, where in each stage biofilm growth on fixed carriers is attained by aeration from the bulk (top-down aeration). In the nitrification step, ammonia nitrogen is oxidized to nitrite by AOB and then nitrate by NOB. Heterotrophic bacteria then generate nitrogen gas by reduction of nitrate or of nitrite in the denitrification step. Recent work has combined these processes into a single stage, via the development of a membrane-aerated biofilm [Satoh *et al.* (2004); Semmens *et al.* (2003)]. In these films, the surface on which biomass grows is a porous polymer through which oxygen can diffuse freely, while all other substrates diffuse to the biomass from the bulk (membrane aeration).

A lack of clear understanding of the roles different bacteria play in nitrogen removal has precluded optimization of both conventional and membrane-aerated reactors. There is

an interest to both understand and eventually control the conditions that lead to optimal community structure and spatial organization, and consequent optimal nitrogen removal. As a step in this direction, this paper simulates the growth of biofilms over a range of substrate conditions, and compares the characteristics of spatial organization that are inherent to top-down- (representing conventional systems) and membrane-aerated (representing single-stage membrane aeration systems) processes.

Materials and methods

Model structure

The simulations were performed on a two-dimensional multi-species multi-substrate cellular automaton (CA)-hybrid model. In a CA-hybrid model, the calculations of substrate levels and of biomass growth are separated. Substrate levels are calculated using discretized forms of the appropriate conservation equations yielding concentration values for each grid element. In contrast, biomass growth is accomplished by treating each bacterium as an object (automaton). Automatons consume substrate at rates calculated by solving the appropriate discrete diffusion/reaction equations, but division, death and detachment are treated as stochastic events. In the model used for this study, the resolution of the model, or the number of bacterial cells in each grid element, is user adjustable.

Model equations. The model equations are shown in Table 1. The first collection of terms in the substrate equations governs diffusion, and the following are multiplicative Monod kinetics terms for consumption and production. The biomass density X^D in the substrate equations is calculated by the fraction of the element occupied by cells multiplied by the cell density, while the value X^I represents the incremental accretion of biomass in the cells following the solution of the diffusion/reaction equations. The parameters b_i are conversions for the mass of oxygen source (O_2, NO_2, NO_3) required per consumption of substrate. The numeric terms in the equations for NO_2 and NO_3 translate the yields $Y_{AOB\text{-}NH4}$ and $Y_{NOB\text{-}NO2}$ into the corresponding amounts of generated nitrite and nitrate metabolite, based on an empirical cell composition of $C_5H_7O_2N$. The parameter $K_{HB\text{-}Flag}$ is an inhibition constant to allow NO_2 and NO_3 consumption by heterotrophs under low oxygen conditions.

Algorithm. The algorithm is based on that of Rittmann *et al.* (2002) or Picioreanu *et al.* (1998). The time derivative is set equal to zero in each of the diffusion-reaction equations and solving the resultant elliptic equation calculates the steady-state consumption rates. These rates are then multiplied through by Δt_{bio} to calculate the substrate consumed during the interval. All erosion, attachment, and cell death events in the model are calculated stochastically, where the probability of occurrence is calculated from a rate parameter, as given in equation [10]. Attachment and erosion are restricted to elements on the biofilm surface. A rudimentary erosion rule was applied, assigning a maximum erosion rate to the highest point above the solid interface in the biofilm, decreasing linearly with height to zero at the solid interface. Cells that "die" become inert biomass. Cell division occurs when a cell accumulates biomass equivalent to the mass of a new bacterial cell. New cells displace an adjacent cell in the direction of least resistance, based on a four-member local neighborhood, which then displaces a further cell in the direction of least resistance, until an empty niche is reached. Following all biofilm events, the diffusion coefficients for each grid element are recalculated based on the fraction of space occupied by biomass, as given in Table 1, and the cycle repeats. The complete algorithm flow is given below:

Table 1 Model equations

$$\frac{\partial[NH_4]}{\partial t} = \nabla(E_{NH_4} \cdot \nabla[NH_4]) - q_{AOB} \cdot X_{AOB} \cdot \frac{[NH_4]}{[NH_4]+K_{AOB \cdot NH_4}} \cdot \frac{[O_2]}{[O_2]+K_{AOB \cdot O_2}} \quad [1]$$

$$\frac{\partial[O_2]}{\partial t} = \nabla(E_{O_2} \cdot \nabla[O_2]) - b_{NH_4 \cdot O_2} \cdot q_{AOB} \cdot X_{AOB} \cdot \frac{[NH_4]}{[NH_4]+K_{AOB \cdot NH_4}} \cdot \frac{[O_2]}{[O_2]+K_{AOB \cdot O_2}} - b_{NO_2 \cdot O_2} \cdot q_{NOB} \cdot X_{NOB} \cdot \frac{[NO_2]}{[NO_2]+K_{NOB \cdot NO_2}} \cdot \frac{[O_2]}{[O_2]+K_{NOB \cdot O_2}} - b_{C \cdot O_2} \cdot q_{HB} \cdot X_{HB} \cdot \frac{[C]}{[C]+K_{HB \cdot C}} \cdot \frac{[O_2]}{[O_2]+K_{HB \cdot O_2}} \quad [2]$$

$$\frac{\partial[NO_2]}{\partial t} = \nabla(E_{NO_2} \cdot \nabla[NO_2]) + \left(1 - \frac{18}{113}\right) \cdot \left(\frac{46}{18}\right) \cdot Y_{AOB \cdot NH_4} \cdot q_{AOB} \cdot X_{AOB} \cdot \frac{[NH_4]}{[NH_4]+K_{AOB \cdot NH_4}} \cdot \frac{[O_2]}{[O_2]+K_{AOB \cdot O_2}} - q_{NOB} \cdot X_{NOB} \cdot \frac{[NO_2]}{[NO_2]+K_{NOB \cdot NO_2}} \cdot \frac{[O_2]}{[O_2]+K_{NOB \cdot O_2}} - \frac{K_{HB \cdot Flag}}{K_{HB \cdot Flag}+[O_2]} b_{C \cdot NO_2} \cdot q_{HB} \cdot X_{HB} \cdot \frac{[C]}{[C]+K_{HB \cdot C}} \cdot \frac{[NO_2]}{[NO_2]+K_{HB \cdot NO_2}} \quad [3]$$

$$\frac{\partial[NO_3]}{\partial t} = \nabla(E_{NO_3} \cdot \nabla[NO_3]) + \left(1 - \frac{46}{113}\right) \cdot \left(\frac{62}{46}\right) \cdot Y_{NOB \cdot NO_2} \cdot q_{NOB} \cdot X_{NOB} \cdot \frac{[NO_2]}{[NO_2]+K_{NOB \cdot NO_2}} \cdot \frac{[O_2]}{[O_2]+K_{NOB \cdot O_2}} - \frac{K_{HB \cdot Flag}}{K_{HB \cdot Flag}+[O_2]} b_{C \cdot NO_2} \cdot q_{HB} \cdot X_{HB} \cdot \frac{[C]}{[C]+K_{HB \cdot C}} \cdot \frac{[NO_3]}{[NO_3]+K_{HB \cdot NO_3}} \quad [4]$$

$$\frac{\partial[C]}{\partial t} = \nabla(E_C \cdot \nabla[C]) - q_{HB} \cdot X_{HB} \cdot \frac{[C]}{[C]+K_{HB \cdot C}} \cdot \frac{[O_2]}{[O_2]+K_{HB \cdot O_2}} - \frac{K_{HB \cdot Flag}}{K_{HB \cdot Flag}+[O_2]} \cdot q_{HB} \cdot X_{HB} \cdot \frac{[C]}{[C]+K_{HB \cdot C}} \cdot \frac{[NO_2]}{[NO_2]+K_{HB \cdot NO_2}} - \frac{K_{HB \cdot Flag}}{K_{HB \cdot Flag}+[O_2]} \cdot q_{HB} \cdot X_{HB} \cdot \frac{[C]}{[C]+K_{HB \cdot C}} \cdot \frac{[NO_3]}{[NO_3]+K_{HB \cdot NO_3}} \quad [5]$$

$$X_{HB}^{I} = \Delta t_{bio} \cdot Y_{HB \cdot C} \cdot q_{HB} \cdot X_{HB} \cdot \left[\frac{[C]}{[C]+K_{HB \cdot C}} \cdot \frac{[O_2]}{[O_2]+K_{HB \cdot O_2}} + \frac{K_{HB \cdot Flag}}{K_{HB \cdot Flag}+[O_2]} \cdot \left(\frac{[C]}{[C]+K_{HB \cdot C}} \cdot \frac{[NO_2]}{[NO_2]+K_{HB \cdot NO_2}} + \frac{[C]}{[C]+K_{HB \cdot C}} \cdot \frac{[NO_3]}{[NO_3]+K_{HB \cdot NO_3}}\right)\right] \quad [6]$$

$$X_{ACB}^{I} = \Delta t_{bio} \cdot Y_{AOB \cdot NH_4} \cdot q_{AOB} \cdot X_{AOB} \cdot \left[\frac{[NH_4]}{[NH_4]+K_{AOB \cdot NH_4}} \cdot \frac{[O_2]}{[O_2]+K_{AOB \cdot O_2}}\right] \quad [7]$$

$$X_{NCB}^{I} = \Delta t_{bio} \cdot Y_{NOB \cdot NO_2} \cdot q_{NOB} \cdot X_{NOB} \cdot \left[\frac{[NO_2]}{[NO_2]+K_{NOB \cdot NO_2}} \cdot \frac{[O_2]}{[O_2]+K_{NOB \cdot O_2}}\right] \quad [8]$$

$$P_{attach} = \frac{r_{attach} \cdot \Delta t_{bio}}{\Delta x^2}; P_{erosion}(h) = \frac{r_{erosion,max} \cdot \Delta t_{bio}}{\Delta x^2} \cdot \frac{h}{h_{max}}; P_{death} = r_{death} \cdot \Delta t_{bio}; D_i = \left(1 - \frac{n_{cell}}{n_{max}}\right) \cdot D_{i,water} + \frac{n_{cell}}{n_{max}} \cdot D_{i,bio}; X_j = n_j \cdot M_{cell} \quad [9-13]$$

(1) Calculate steady state substrate concentrations and consumption rates.
(2) Calculate changes to the biofilm due to attachment or erosion.
(3) Calculate changes to the biofilm due to cell division.
(4) Calculate changes to the biofilm due to cell death.
(5) Recalculate diffusion coefficients for grid elements, and return to step 1.

The elliptic equations were discretized by a central difference approximation and solved iteratively using Newton's method. The nonlinear diffusion coefficient was approximated by the diffusion coefficient of the central grid element in each difference term. Periodic boundary conditions were applied in the x-direction. All concentrations were set to the bulk concentration at the upper boundary and a zero-flux condition was applied at the solid interface, with the exception of oxygen in the membrane-aeration cases in which an influent oxygen concentration was specified.

Parameter estimation. All unmarked organism parameters in Table 2 are adapted from Rittmann *et al.* (2002) and expressed in mg of COD per mg substrate where appropriate. Parameters marked with a $*$ are taken from Marazioti *et al.* (2002). The extinction coefficient marked with a $**$ is assumed. All diffusion coefficients are for water and were taken from the *Handbook of Chemistry and Physics*, 81st edition, where that of the carbon source is taken as that for acetic acid. Diffusion coefficients in the biofilm were assumed to be one half of those in the liquid.

Simulations. A set of 128 simulations was performed which varied bulk ammonia from 2 to 8 mg/L, bulk oxygen from 2 to 8 mg/L, and bulk carbon from 0 to 6 mg/L in increments of 2 mg/L at low erosion rates ($r_{\text{erosion,max}} = 0.1\ \text{mg/m}^3\text{d}$) and no attachment for 12 days under both top-down and membrane-aeration conditions. All simulations were cultured from the same "seed" file, created by running the simulator for 0.5 days under conditions of no erosion and high attachment rate ($r_{\text{attach}} = 10\ \text{mg/m}^3\text{/d}$), and bulk ammonia, oxygen, and carbon concentrations all held at 0 mg/L.

Results and discussion

Shown in Figure 1 are the time profiles of biofilms grown at substrate condition A (NH_4 4 mg/l, O_2 4 mg/l, carbon 4 mg/l) under top-down and membrane-aeration conditions, respectively. The top-down aeration run in Figure 1A is characterized by growth of AOB and heterotrophs in the direction of higher concentrations of their respective substrates, and of oxygen. The result is that dense, active biomass at the surface slowly grows on an

Table 2 Model parameters

Organism parameters				Other parameters		
	AOB	NOB	HB		Description	Value
$Y_{X/S}$ (mg /mg S)	0.47	0.16	0.64	n_{max}	Number of cells per grid element	8
q_X (mg /mg d)	2.18	6.55	2.11	P_{cell}	Cell density (mg/l)	30,000
$K_{X\text{-}O2}$ (mg/l)	0.5	0.68	0.1	X	Width of simulation (elements)	100
$K_{X\text{-}S}$ (mg/l)	1.5	2.7	1.25	δ_b	Concentration boundary layer (cm)	4.00×10^{-3}
r_{death} (/d)	0.05	0.05	0.05	M_{cell}	Bacterial cell mass (mg)	9.50×10^{-10}
$K_{X\text{-}NO2}$ (mg/l)	–	–	0.28 $*$	E_{NH4}	Ammonia diffusion coefficient (m^2/s)	1.96×10^{-9}
$K_{X\text{-}NO3}$ (mg/l)	–	–	0.77 $*$	E_{O2}	Oxygen diffusion coefficient (m^2/s)	2.03×10^{-9}
$K_{HB\text{-}Flag}$ (mg/l)	–	–	0.1 $**$	E_{NO2}	Nitrite diffusion coefficient (m^2/s)	1.91×10^{-9}
				E_{NO3}	Nitrate diffusion coefficient (m^2/s)	1.90×10^{-9}
				E_C	Carbon diffusion coefficient (m^2/s)	1.20×10^{-9}
				Δx	Grid scale (m)	6.33×10^{-6}
				Δt_{bio}	Timescale for changes to biofilm (d)	0.1

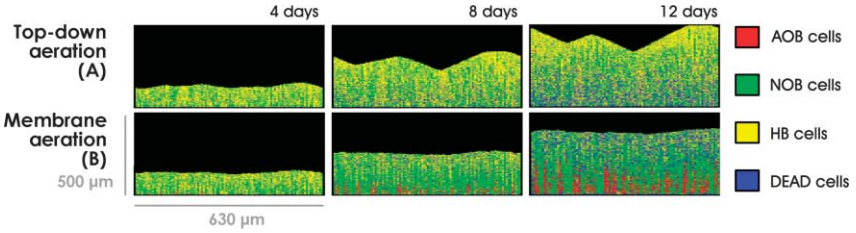

Figure 1 Biofilm growth profiles to 12 days

accumulating base of inert biomass toward the biofilm–solid interface. The upward-reaching growth in the direction of high substrate concentration also leads to uneven, column-like biomass formation. NOB are not present to any significant degree within the film. NOB have a lower affinity for oxygen than either AOB or heterotrophs, and are unable to compete effectively for it even after significant levels of its substrate nitrite have accumulated.

The structure of the biofilm in the membrane-aeration run (1B) differs significantly from that of the top-down run in several respects. Physically, the biofilm surface is much more uniform and flat. At least initially, growth occurs most rapidly in the zone where high substrate concentration overlaps high oxygen concentration, i.e. close to the biofilm–membrane interface, reflected in the accumulation of inert biomass near the surface. As growth progresses, nitrite accumulates as a metabolic byproduct of the AOB. Figures 2A and B show the averaged substrate profiles with depth for the two runs in Figures 1A and B at 12 days. The heterotrophs are capable of utilizing nitrite in place of oxygen, and thus in the membrane-aerated films are free to grow farther from the membrane interface as the nitrite accumulates. A second shift in spatial organization occurs when the localization of high levels of nitrite near the aerated surface creates a niche in which NOB can compete for oxygen. The NOB then begin to displace AOB from the bottom layers of the biofilm so that three distinct zones appear – a central zone dominated by AOB, below which NOB flourish, and above which heterotrophs are growing amidst an accumulation of inert biomass. Thus in membrane-aerated biofilms nitrification appears to occur via an inner layer of autotrophic bacteria, followed by diffusion of the metabolic nitrite and nitrate products to an outer layer of heterotrophic denitrifiers.

Effect of substrate concentration on spatial distribution. Figure 3 shows the NOB, AOB, and heterotroph cell count at 12 days for the set of simulations described in the Methods section. The radius of the sphere at each point is proportional to the cell count, with a unit radius being equal to the maximum value obtained in either the top-down or membrane aeration condition. This model finds no significant niche for NOB within the substrate ranges of the study for top-down aeration, while it does for membrane aeration, emerging with increasing oxygen and ammonia concentration in the bulk. A set of repetitions on substrate condition A using randomized seed files showed this effect to be significant at 95% confidence (data not shown). Since NOB are known to be found in top-down aerated biofilms, it should be stressed that the simplicity of the model makes it sufficient only to reveal the emergence of this particular NOB niche and does not prove or disprove the presence of other potential niches in real biofilms. Convective flow, biofilm architecture, as well as natural diversity in the substrate affinities and growth rates of bacteria are all factors unexamined by this model. A surprising result, illustrating the limitations of the model, is seen in the marked decrease of heterotroph growth with increasing ammonia level. This model employs a simple "path of least resistance" algorithm to govern the movement of dividing bacteria, so that as the bulk ammonia

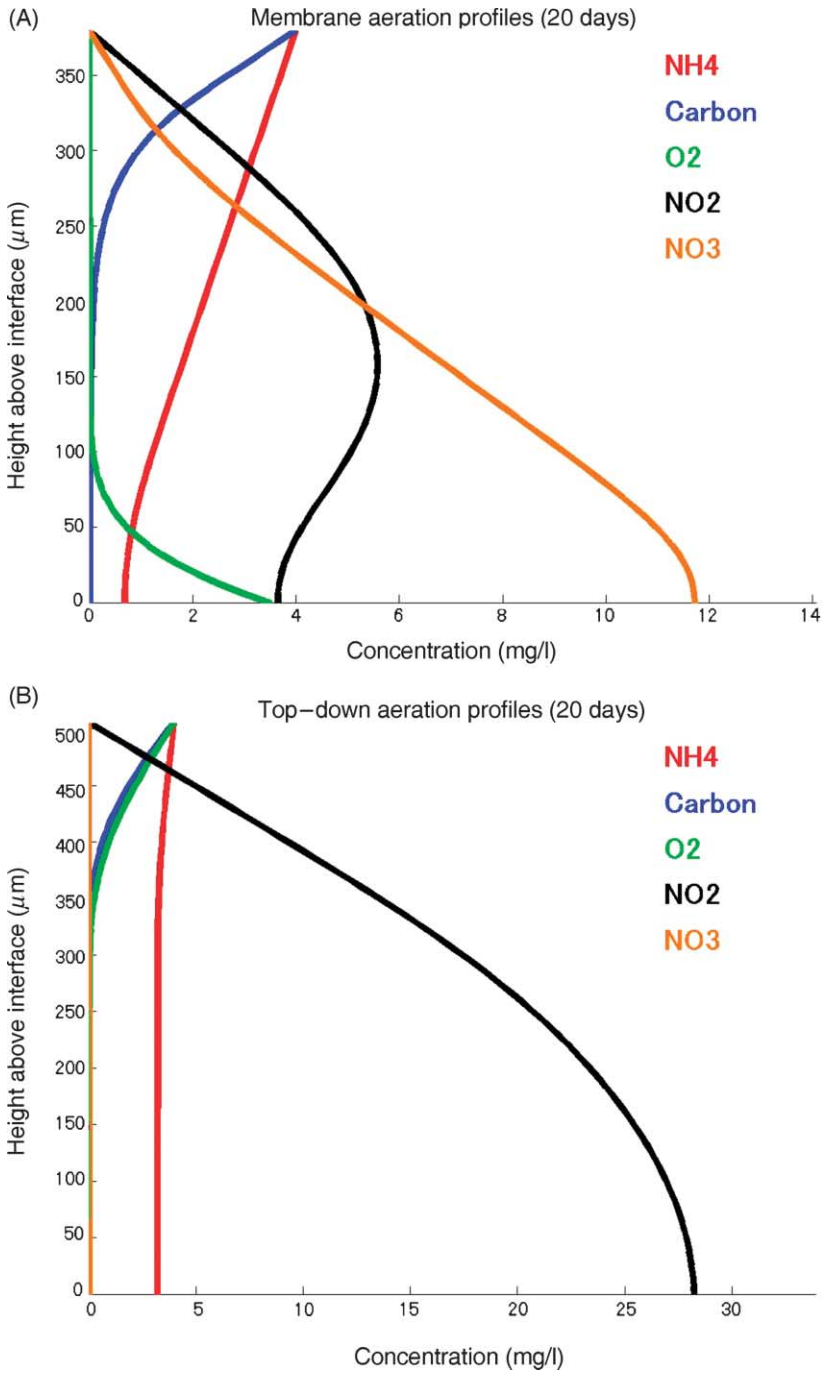

Figure 2 Substrate profiles at day 12 under substrate condition A

concentration increases (effectively, as the aggregate growth of AOB and NOB increases relative to that of the heterotrophs) the region near the surface where the heterotrophs grow becomes noisy and unstable. Intuition tells us that higher AOB and NOB growth leads to higher nitrite and nitrate levels, and thus higher levels of heterotroph growth. Model development accounting for bacterial aggregation in the biofilm would disallow such simple mixing.

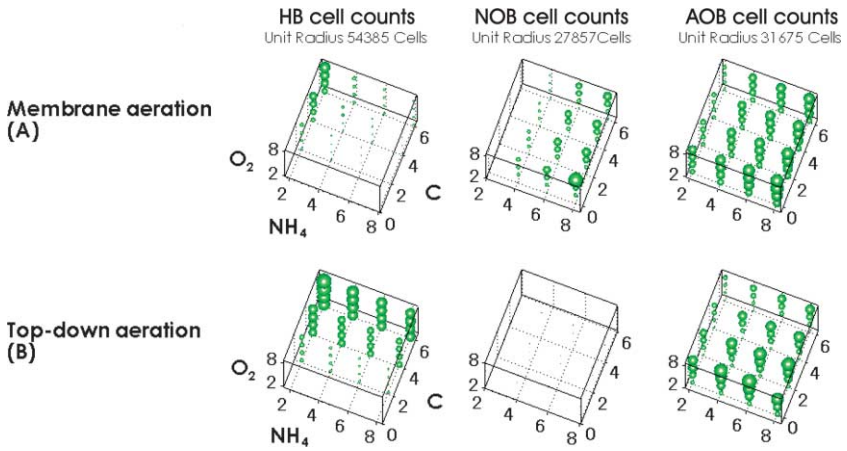

Figure 3 AOB, NOB, and heterotroph cell counts as a function of bulk ammonia, oxygen, and carbon

Implications for wastewater treatment. These results illustrate that mechanisms exist by which NOB can compete more effectively for oxygen and substrate in a membrane-aerated biofilm than in a system with top-down aeration. The overlap of high oxygen and nitrite concentrations that emerges near the membrane–biofilm interface under membrane aeration creates a niche in which NOB can compete effectively for substrate and oxygen, whereas no such niche exists under top-down aeration. This has significance for single-stage nitrifying–denitrifying reactor systems. The growth of significant NOB means that a significant fraction of the nitrogen is shunted to nitrate by NOB metabolic activity. This can impact the treatment of inorganic wastewater, where metabolism of nitrate requires more carbon input than that of nitrite and thus represents an increase in costs.

Clearly, the effectiveness of wastewater treatment is influenced proximately by the organization of bacterial communities in the biofilm, which in turn is a function of the reactor conditions. To improve performance in such systems, it is important to analyze this spatial organization over a wide range of conditions and reactor configurations. However, the time and costs associated with reactor operation and analysis via microbial techniques make such study impractical. The simple 2D model used in this study facilitated qualitative analysis of bacterial community structure quickly and reproducibly, and illustrates the applicability of numerical analysis to improving reactor performance.

Conclusions

This study compared top-down and membrane-aeration approaches for the removal of nitrogen from wastewater by simple numerical simulation, and found major differences in spatial organization between the two. In particular, an inner layer of autotrophic nitrifiers and an outer layer of heterotrophic denitrifiers arose under membrane-aeration conditions. The community structure was also found to change dramatically, and to be sensitive to changes in substrate conditions, which can impact overall nitrogen removal efficiency. The effectiveness of the model used in this study in looking qualitatively at differences in community structure and spatial organization illustrates the role that such models can play in analyzing such structure in order to improve reactor performance.

References

Aoi, Y., Miyoshi, T., Okamoto, T., Tsuneda, S., Hirata, A., Kitayama, A. and Nagamune, T. (2000). Microbial ecology of nitrifying bacteria in wastewater treatment process examined by fluorescence in situ hybridization. *J. Biosci. Bioeng*, **90**(3), 234–240.

Hand book of chemistry and Physics (2000) ed. D.R. Lide, 81st edn, CRC Press. Boca Raton, USA

Marazioti, C., Kornaros, M. and Lyberatos, G. (2002). Kinetic modeling of a mixed culture of *Pseudomonas denitrificans* and *Bacillus subtilis* under aerobic and anoxic operating conditions. *Wat. Res.*, **37**, 1239–1251.

Okabe, S., Satoh, H. and Watanabe, Y. (1999). In situ analysis of nitrifying biofilms as determined by in situ hybridization and the use of microelectrodes. *Appl. Env. Microbiol.*, **65**, 3182–3191.

Picioreanu, C., van Loosdrecht, M.C.M. and Heijnen, J.J. (1998). Mathematical modeling of biofilm structure with a hybrid differential-discrete cellular automaton approach. *Biotech. Bioeng.*, **58**(1), 101–116.

Rittmann, B.E., Stilwell, D. and Ohashi, A. (2002). The transient-state, multiple-species biofilm model for biofiltration processes. *Wat. Res.*, **36**, 2342–2356.

Satoh, H., Ono, H., Rulin, B., Kamo, J., Okabe, S. and Fukushi, K. (2004). Macroscale and microscale analyses of nitrification and denitrification in biofilms attached on membrane aerated biofilm reactors. *Wat. Res.*, **38**, 1633–1641.

Schramm, A., Larsen, L.H., Revsbech, N.P., Ramsing, N.B., Amann, R. and Schleifer, K. (1996). Structure and function of a nitrifying biofilm as determined by in situ hybridization and the use of microelectrodes. *Appl. Env. Microbiol.*, **62**, 4641–4647.

Semmens, M., Dahm, K., Shanahan, J. and Christianson, A. (2003). COD and nitrogen removal by biofilms growing on gas permeable membranes. *Wat. Res.*, **37**, 4343–4350.